Journal of Cleaner Production 489 (2025) 144679

Contents lists available at ScienceDirect

Journal of Cleaner Production

journal homepage: www.elsevier.com/locate/jclepro

Exploration of biomass ashes (BA) to decontaminate highly metal-rich acid mine drainages (AMDs): Column and batch experiments

Carlos R. Cánovas [a,*], Gerardo A. Amaya-Yaeggy [a], Dileesha Jayahansani Kotte-Hewa [b,c], Rafael Pérez-López [a], Francisco Macías [a], Rafael León [a], José Miguel Nieto [a], María Dolores Basallote [d]

[a] Department of Earth Sciences & Research Center on Natural Resources, Health and the Environment, University of Huelva, Campus "El Carmen", E-21071, Huelva, Spain
[b] KU Leuven, Department of Soil and Water Management, Kasteelpark Arenberg 20, 3001, Heverlee, Belgium
[c] Belgian Nuclear Research Centre, SCK CEN, Boeretang 200, Mol, 2400, Belgium
[d] Department of Ecology and Coastal Management, Institute of Marine Sciences of Andalusia (ICMAN-CSIC), E-11510, Puerto Real, Spain

ARTICLE INFO

Handling Editor: Tomas B. Ramos

Keywords:
Circular economy
Acid mine drainage
Passive treatment
Active treatment
Biomass ashes

ABSTRACT

This work investigates the suitability of biomass ash (BA), a waste generated after biomass burning, as alkaline material to treat highly acidic (pH 1.9–2.0) and metal rich acid mine drainages (AMD). To address this issue, batch (at solid:liquid ratios of 1:2, 1:5; 1:10, 1:20, 1:100 and 1:200) and column experiments were performed. During batch experiments, the contact of AMD with BA provoked an intense increase of pH values, especially at higher S:L ratios (1:2 and 1:5), i.e., from 1.9 to 7.3 and 6.4, respectively, due to the alkalinity provided by BA, which led to strong removal of dissolved metal/loids (e.g., 89–99 % of Fe, 99% of Al, Cu and As, 75–99% of Pb) and sulfate (66–68%) for both ratios. The removal efficiency obtained using intermediate and low S:L ratios was remarkably lower for most metal/loids except for As, with values above 95% at the end of the experiment for all S:L ratios. On the other hand, the dissolution of metal oxides, initially contained in BA, led to the release of elements commonly found associated to these oxides in BA (e.g., Al, Ca, Mg, K, Na, Sr, or P). The removal rates obtained in column experiments were lower, due to the fast depletion of alkalinity during the first days of the experiment, which make columns less suitable for AMD treatment than batch reactors. A removal of 100% of Cu, As, V and Ga, 99% of Pb, 73% of Fe and Cd, 64% of Zn and Co, and 60% of sulfate was achieved after 24 h. However, the efficiency of the column decreased progressively to the end of the experiment, reaching similar values than in input waters, except in the case of As (around 91% of removal), due to the preferential sorption of oxyanions ($H_2AsO_4^-$ and $HAsO_4^{2-}$). The precipitation of schwertmannite and to a lesser extent jarosite, and sorption processes on these minerals, are the main process controlling metal retention in both batch and column experiments. Despite the low alkalinity of the BA used, the removal rates of metal (loid)s were significant, and hence, it constitutes a promising option to treat AMD in mining areas worldwide where this waste is generated.

1. Introduction

Sulfide mining activities often result in the generation of acid mine drainage (AMD), a significant environmental concern worldwide characterized by the release of acidic and metal-laden waters into surrounding ecosystems. The global distribution of AMD was highlighted by Johnson and Hallberg (2005) who estimated that in 1989, around 19,300 km of rivers and 720 km^2 of lakes and reservoirs were severely affected by AMD worldwide. The growing mining activities developed during the last years to satisfy the increasing demand of raw materials may have aggravated these impacts. There are significant examples of AMD affection across the world. Ziemkiewicz et al. (2003) estimated around 20,000 km of AMD-affected streams in USA. In the case of Australia, considered as the world's leading exporter of minerals, it is estimated that AMD affects about 21,500 km^2 of land (Naidu et al., 2019). The generation of mine waters in China has been estimated to be around 7 billion m^3 per year (He et al., 2018), of which AMD may account for more than 50 % of the total (Cai, 2015). In the case of the

* Corresponding author.
E-mail address: carlos.ruiz@dgeo.uhu.es (C.R. Cánovas).

https://doi.org/10.1016/j.jclepro.2025.144679
Received 25 September 2024; Received in revised form 23 December 2024; Accepted 3 January 2025
Available online 6 January 2025

Iberian Pyrite Belt (IPB, SW Iberian Peninsula), one of the largest deposits of massive sulfides in the world, it is estimated a generation of around 25 million m^3/yr of AMD, which causes the pollution of the Tinto and Odiel fluvial basins, contributing with up to 0.8% of the global gross flux of Cu and 2.8% of Zn delivered by worldwide rivers to oceans (Nieto et al., 2013).

AMD poses severe risks to aquatic life and can have far-reaching ecological consequences; therefore, the adoption of effective and sustainable treatment methods is required to avoid or mitigate these potential impacts. Mine waters can be treated by different types of technologies, which can be grouped into active and passive treatments (Johnson and Hallberg, 2005). Active treatments require energy consumption and continuous addition of chemical reagents, while passive treatments use the sources of renewal energy (e.g., gravity, energy of microbial metabolism, photosynthesis or energy released from geochemical reactions; Akcil and Koldas, 2006). In addition, passive treatments require scarce maintenance unlike active treatment. For these reasons, active treatments are commonly used in operating mines as large volumes of water need to be treated prior to discharge, whereas passive treatments are more suitable for abandoned mines or during the remediation programs after mine closure (Johnson and Hallberg, 2005). Although passive treatments such as reactors, wetlands, limestone drains or disperse alkaline substrate (DAS) systems (Gotore et al., 2025; Kotte-Hewa et al., 2023) are more environmentally friendly and cost-effective than active treatments, the use of chemical reagents (e.g., calcite and dolomite) involves significant cost and environmental impacts during its manufacturing. Therefore, a more sustainable and cost-effective approach needs to be applied, based on the use of alkaline waste materials. One promising approach involves the utilization of biomass ash (BA), a byproduct of biomass combustion, as a remediation agent. BA is rich in alkaline compounds, such as calcium carbonates and oxides, which can neutralize the acidity of AMD and precipitate metal ions. This material has been successfully used for the treatment of highly acid effluents from the fertilizer industry, with removal rates of 87–100% for Fe, U, F and Cr, and around 50% for Al, Zn, Cu and As (Millán Becerro et al., 2020) and for the recovery of rare earth elements (REE) from AMD, with removal values of 99% (Kotte-Hewa et al., 2023). Bogush et al. (2019) also investigated the removal of metals from synthetic AMDs, using BA from straw, meat and bone meal, and poultry litter combustion, achieving satisfactory results. The impact of BA generated during wildfires on the improvement of acidic waters has been even reported in watersheds affected by mining (Romero-Matos et al., 2023). However, the use of BA in extremely metal rich AMD waters has not been explored, and this type of mine waters is responsible of most metal pollution in abandoned metal mine districts worldwide (Moreno-González et al., 2020), therefore the potential application of this waste material as neutralizing agent could be a promising solution to degraded historical mining areas.

Therefore, it seems evident that the mechanisms behind metal removal from highly metal-rich AMDs using BA should be further investigated. By examining the chemistry of the neutralization process and the interactions between BA and acidic mine waters, we aim to elucidate the feasibility and efficacy of this innovative treatment method. Unlike other waste materials, the neutralization of AMD with BA has been scarcely studied in literature. The research objectives of this work are i) to determine the suitability of using BA as neutralizing material to treat AMD and ii) to study the geochemical factors controlling the solubility of contaminants during the treatment with BA. The results obtained in this study may contribute to the development of sustainable and efficient strategies for managing AMD in mining-affected regions in the world.

2. Methods

2.1. Material sampling and characterization

BA samples (5 kg) were collected from the biomass electricity complex of ENCE (50 MW) at Huelva (SW Spain). This complex generates around 56,000 ton/yr of ash, close to the main AMD sources of the IPB (about 100 km away), which would reduce the transporting costs of this alkaline byproduct. This material was chemically characterized after total acid digestion at the Research Services of the University of Huelva using Inductively coupled plasma atomic emission spectroscopy (ICP-AES; Jobin Yvon Ultima 2) for major elements and Inductively Coupled Plasma Mass Spectrometry (ICP-MS; Agilent 7700) for trace elements. The detection limits were 0.3 mg/L for S; 0.1 mg/L for Na; 0.1 mg/L for Fe, K, Mg, and Si; 0.02 mg/L for Al and Ca; and 2 μg/L for trace elements. The analytical precision was assessed by triplicate analyses of selected samples with values below 5% in all cases. Blanks were also analyzed in each analysis sequence, with all elements below the detection limit. The analytical accuracy was evaluated by the analysis of reference materials (NIST-1640) and home-made solutions, with differences below 7% between these and the referenced concentrations. Solid samples were also mineralogically characterized before starting and after ending the experiments. The mineralogical composition of solid samples was determined by X-ray diffraction (XRD) at the R + D Services of the University of Huelva using a Bruker D5005 X-ray diffractometer employing Cu Ka radiation. The selected settings were 40 kV, 30 mA, a scan range of 3–65° 2Θ, 0.02° 2Θ step size, and 2.4 s counting time per step. The samples were examined under a JEOL JSM-IT500HR Field Emission Scanning Electron Microscope coupled with Oxford XMax 150 Energy Dispersive System (FESEM-EDS) at the Research Services of the University of Huelva.

In order to perform the experiments, around 25 L of acidic and metal-rich AMD was collected from Poderosa Mine (Huelva, Spain), one of the most pollutant sources of the Odiel River, which exhibits a high variability. For example, the dissolved Fe pollutant load released through the mine gallery ranges from ~100 to 200 kg/day of Fe during base flow to almost 2200 kg/day during the flow peak (Cánovas et al., 2018). For practical purposes, samples for batch and column experiments were collected on different periods of the year. To determine the chemical composition of the water, samples were filtered (through 0.22 μm), acidulated to pH < 1 with ultrapure HNO_3 and refrigerated until analysis. Different physico-chemical parameters such as temperature, pH, electrical conductivity (EC) and oxidation-reduction potential (ORP) were measured using a CRISON MM40+ equipment. A three-point calibration was performed for both EC and pH (147, 1413 μS/cm and 12.88 mS/cm, and 4.01, 7.00 and 9.21, respectively), while the ORP was controlled using two reference solutions (240 and 470 mV). The ORP values were corrected to obtain the potential referred to the hydrogen electrode (Nordstrom and Wilde, 1998). Both materials (BA and AMD) were used without prior treatment.

2.2. Batch and column experiments

Two different approaches were followed to study the suitability of BA to be used as a remediation reagent of highly-acidic and metal-rich AMD waters. Batch experiments were performed using 6 different solid:liquid ratios (1:2, 1:5, 1:10, 1:20, 1:100 and 1:200) to optimize the addition of BA. Kinetic aspects were also evaluated considering different reaction times for each experiment (15 min, 1 h, 3 h, 6 h, 12 h, 24 h, 48 h and 96 h). Samples were stirred during the experiment, and samples corresponding to each reaction time were removed, centrifuged and the supernatant was filtered through 0.22 μm cellulose nitrate filters and acidified with ultrapure HNO_3 before analysis. Physico-chemical variables (pH, ORP, EC and temperature) were measured in each sample following the abovementioned procedure.

Column experiments were also performed, consisting of an initial

Table 1
Chemical composition of biomass ashes used in the experiments.

Biomass ashes composition			
(%)		mg/kg	
SiO_2	67.3	Sr	209
Al_2O_3	11.3	V	127.0
CaO	8.45	Cu	77
K_2O	4.83	Zn	50
Fe_2O_3	4.69	Cr	29
MgO	1.47	As	20
P_2O_5	0.93	Ni	17
Na_2O	0.67	Y	9.3
TiO_2	0.20	Pb	8
MnO	0.10	Ga	5.9
SO_3	0.04	Co	5.5

tank (5 L) to store AMD waters, connected to a column with a peristaltic pump at a constant rate of 0.3 mL/min. The columns made of HDPE (6 cm of diameter and 40 cm length) were filled with BA mixed with wood shaving (20%:80%) to provide porosity, following the Dispersed-Alkaline Substrate (DAS) technology proposed for the passive treatment of AMD in the IPB (Macías et al., 2012). The column bottom was filled with 3 cm of silica sand to enhance drainage. The column was connected to a settling pond (445 cm^3) to store the treated waters and allow flocculation and sedimentation of precipitated minerals. Column experiments lasted 25 days, where samples were collected at a variable frequency (daily the first week and every 2–3 days the remaining time), following the same procedure as for batch experiments (i.e., measure of physico-chemical parameters, filtration, acidification, and analysis). Once finished, the column was dismantled, and solid samples were collected and processed for mineralogical analysis.

2.3. Geochemical modelling and statistical analysis

Metal speciation and saturation indices of waters were obtained using the PHREEQC code v3.73 (Parkhurst and Appelo, 2013). The Minteq v4 database was enlarged with the thermodynamic data from schwertmannite (Yu et al., 1999) and other minerals (e.g. melanterite, copiapite, coquimbite) from other databases provided by the code. A Principal Component Analysis (PCA) has been performed on batch and column samples to infer behavior patterns in selected variables. PCA allows reducing the number of variables in a multivariate data set but retaining as much as possible of the variation present in the data set. Variables were standardized to z-scores to fit a normal distribution; thus the Pearson (n-1) correlation matrix was used (Davis, 2002).

3. Results and discussion

3.1. Characterization of starting materials

BA used in the experiments are mainly composed of Si (67 wt% SiO_2), Al (11 wt% Al_2O_3), Ca (8.5 wt% CaO), K (4.8 wt% K_2O), Fe (4.7

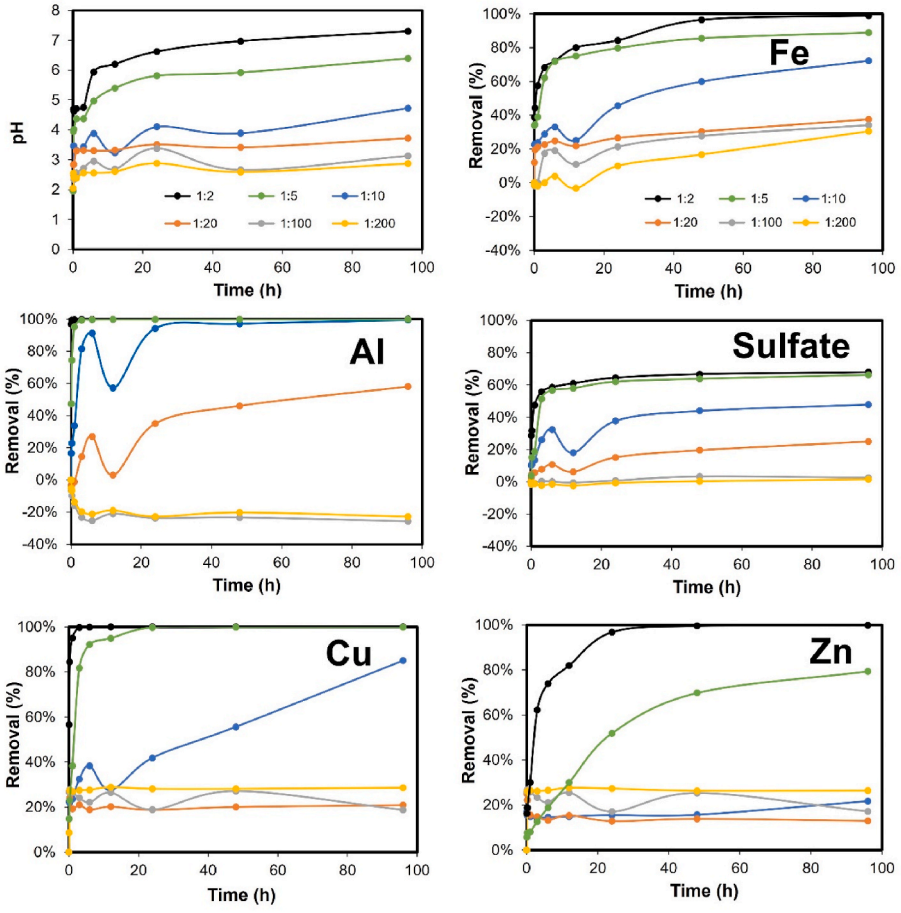

Fig. 1. Evolution of solution pH and removal efficiency of common AMD contaminants during the batch experiments using BA.

Table 2
Chemical composition of acid mine waters (AMD) used to perform the batch and column experiments.

AMD batch			
mg/L		µg/L	
pH	1.95	**Mn**	4571
EC (mS/cm)	8.4	**As**	2415
Eh (mV)	486	**Co**	1115
Fe	1633	**Cd**	327
Al	337	**Pb**	191
Sulfate	6909	**V**	132
Cu	101	**Ni**	102
Zn	84	**Ga**	61
Ca	121	**Tl**	37
Si	38	**Sb**	31
K	14	**Sc**	20
Phosphate	3.1	**Cr**	10
AMD column			
mg/L		µg/L	
pH	2.04	**Mn**	79812
EC (mS/cm)	14.1	**As**	12525
Eh (mV)	450	**Co**	11200
Fe	6111	**Cd**	1553
Al	906	**Pb**	169
Sulfate	19371	**V**	837
Cu	193	**Ni**	2603
Zn	748	**Ga**	73
Ca	211	**Ge**	74.0
Si	62	**Sb**	5.0
K	7.1	**Sc**	38
Phosphate	5.8	**Cr**	637

wt% Fe_2O_3) and Mg (1.5 wt% MgO), with high concentrations of other elements such as P (0.93 wt% P_2O_5), Na (0.67 wt% Na_2O), Ti (0.20 wt% TiO_2), Mn (0.10 wt% MnO), and S (0.04 wt% SO_3) (Table 1). According to the Vassilev classification (Vassilev et al., 2013), this BA would be of S type, characterized by being rich in Si, Al, Fe, Na and Ti oxides, with around 84% of these compounds, compared to the low contents of C type (10% of Ca, Mg and Mn oxides) and PK type components (5% of K, P, S and Cl oxides). This means that these BA have a high acid tendency, which provides a lower potential to treat AMD waters compared to other low and/or medium acid tendency types such as C, PK and mixed types (Bogush et al., 2019). In addition, the BA used in the experiments have significant concentrations of trace elements such as Sr (209 mg/kg), V (127 mg/kg), Cu (77 mg/kg), Zn (50 mg/kg), Cr (29 mg/kg), As (20 mg/kg), Co (17 mg/kg), Y (9.3 mg/kg), Pb (8.0 mg/kg), Ga (5.9 mg/kg) or Ni (5.5 mg/kg) (Table 1). This material showed a low crystallinity, and only quartz was detected in XRD patterns. An examination by FESEM revealed the presence of different oxides of Si, Ca, Mg, Na, Fe, Al and K (Fig. S1).

The AMD used for the batch experiments exhibited pH values below 2 (Table 2), EC values of 8.4 mS/cm and elevated concentrations of sulfate (6909 mg/L), Fe (1633 mg/L), Al (337 mg/L), Cu (101 mg/L), Zn (84 mg/L) and minor concentrations of other trace metal/loids (e.g., 4.5 mg/L of Mn, 2.4 mg/L of As, 1.1 mg/L of Co, 0.33 mg/L of Cd or 0.19 mg/L of Pb; Table 2). On the other hand, AMD samples used for column experiments exhibited a very low pH value (2.05) and higher EC (14 mS/cm) values than those used in batch experiments, with high concentrations of sulfate (20814 mg/L), and metal/loids (e.g., 6664 mg/L of Fe, 910 mg/L of Al, 794 mg/L of Zn, 196 mg/L of Cu and 14 mg/L of As). According to the Ficklin diagram, these waters can be classified as high acid-extreme metal waters. This diagram is commonly used to categorize

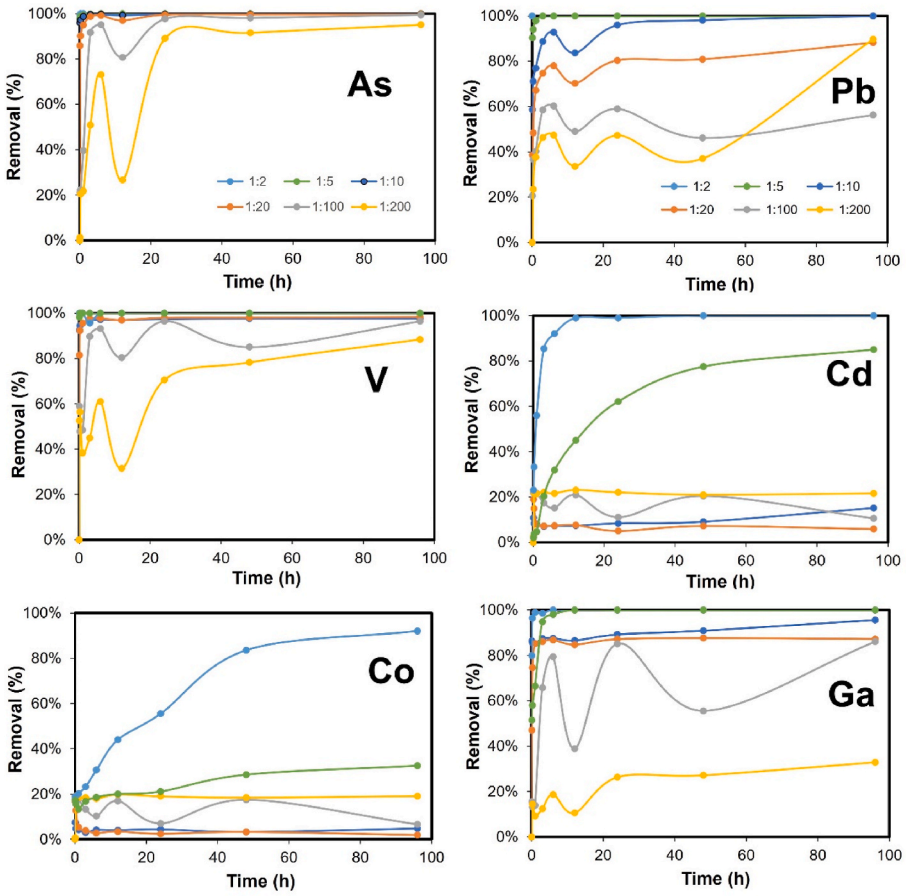

Fig. 2. Evolution of removal efficiency of trace elements commonly found in AMD during the batch experiments using BA.

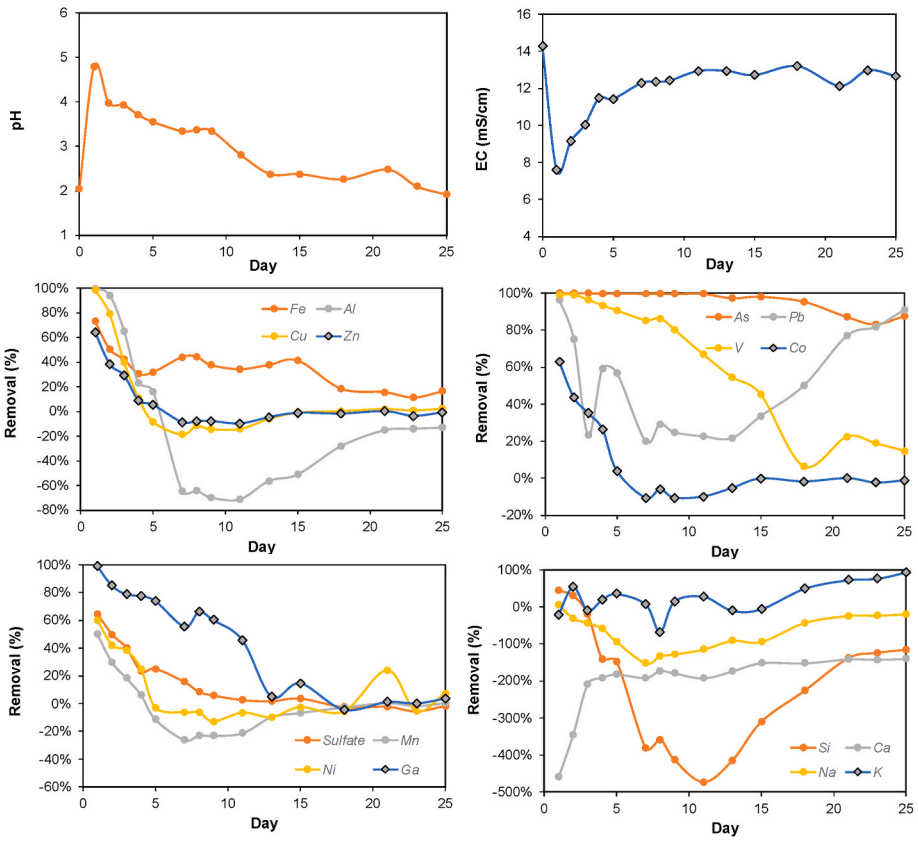

Fig. 3. Evolution of solution pH, electrical conductivity (EC) and removal efficiency of selected AMD contaminants at the outlet of batch experiments using BA.

AMD waters according to their pH and base metal concentrations (Ficklin et al., 1992).

3.2. Batch experiments

The contact of AMD with BA caused a sharp increase of pH values, especially at higher S:L ratios (1:2 and 1:5), from 1.9 to 4.7 and 4.3, respectively, within the first hour of the experiment (Fig. 1), due to the alkalinity provided by BA. At intermediate ratios (1:10 and 1:20), the increase was also notable, from 1.9 to 3.3. The pH values exhibited an increasing tendency towards the end of the experiment (7.3 and 6.4 for ratios 1:2 and 1:5, 4.7 and 3.7 for ratios 1:10 and 1:20 at 96 h; Fig. 1). At lower ratios (1:100 and 1:200), the increase was lower during the experimental run, reaching values of 3.4 and 2.1 at the end, respectively, due to the scarce alkalinity supplied by both ratios. In the case of the total dissolved solids (TDS), a significant decrease was also observed through the experiment. For example, a progressive removal efficiency was observed for Fe during the experiment, especially at higher S:L ratio (Fig. 1). Thus, the removal of Fe at 1:2 and 1:5 ratios ranged from 34 to 33% (5 min) to 99 and 89%, respectively, at the end of the experiment (96 h). On the other hand, a declining tendency for Fe removal was observed with the decrease in S:L ratios; 72% for S:L ratio of 1:10, 37% for 1:20, 34% for 1:100 and 33% for 1:200 at the end of the experiment (Fig. 1).

A similar evolution was observed for the rest of major AMD contaminants (i.e., Al, sulfate, Cu and Zn), although with some remarkable differences. In the case of Al and Cu, the nearly total removal of both elements was achieved at the beginning of the experiment using high S:L ratios (1:2 and 1:5). High removal rates were also obtained using a S:L ratio of 1:10 for Al and Cu (99 and 83%, respectively), however, the removal rates using lower ratios were of minor importance. Even, the concentration of dissolved Al in solution increased at lower ratios (1:100 and 1:200) with respect to initial values due probably to the dissolution of Al oxides, initially contained in BA. The dissolution of other oxides resulted in sharp increases in concentration of elements commonly found associated to oxides in BA (e.g., Ca, Mg, K, Na, Sr, or P; Fig. S2), although the fluctuation of values during the experiment suggests the existence of re-precipitation processes in other mineral phases. It is also remarkable the lower performance for Zn removal obtained using the S:L ratio of 1:5 (77%) compared to 1:2 (100%; Fig. 1). On the other hand, the lowest performance was observed for sulfate removal, with values comprising 66–68% using high S:L ratios (1:2 and 1:5), 24–48% for intermediate ratios (1:10 and 1:20) and only around 2% for lower ratios (1:100 and 1:200). However, considering the high starting sulfate concentrations (6909 mg/L; Table 2), high contents of sulfate were removed in total from the solution. These removal values may be however masked by the occurrence of these metals in BA (Table 1), which could be released during the interaction of BA with the acidic waters.

Although other metal/loids (e.g., As, Pb, Cd, V, or Ni) are found at lower concentrations in AMD, they should be removed due to their toxic effects. Fig. 2 shows the removal efficiency for selected trace metals using BA in batch experiments. As can be seen, BA turned to be very effective in the removal of As, with values above 95% at the end of the experiment for all S:L ratios considered. Similar results were also recorded for Pb, V, and Ga with values above 90, 88% and 86%, respectively (except for Pb at a S:L ratio of 1:100 and Ga at 1:200). However, a sharp decrease in the removal efficiency of these elements was observed at around 16 h (Fig. 2), which may indicate the existence of geochemical reactions, releasing them back to solution, especially at lower S:L ratios. On the other hand, the removal of other trace metals such as Cd, Co and Ni was only successful at the higher S:L ratios (especially at 1:2).

3.3. Column experiments

The BA contained in the column caused a sharp increase of pH in the

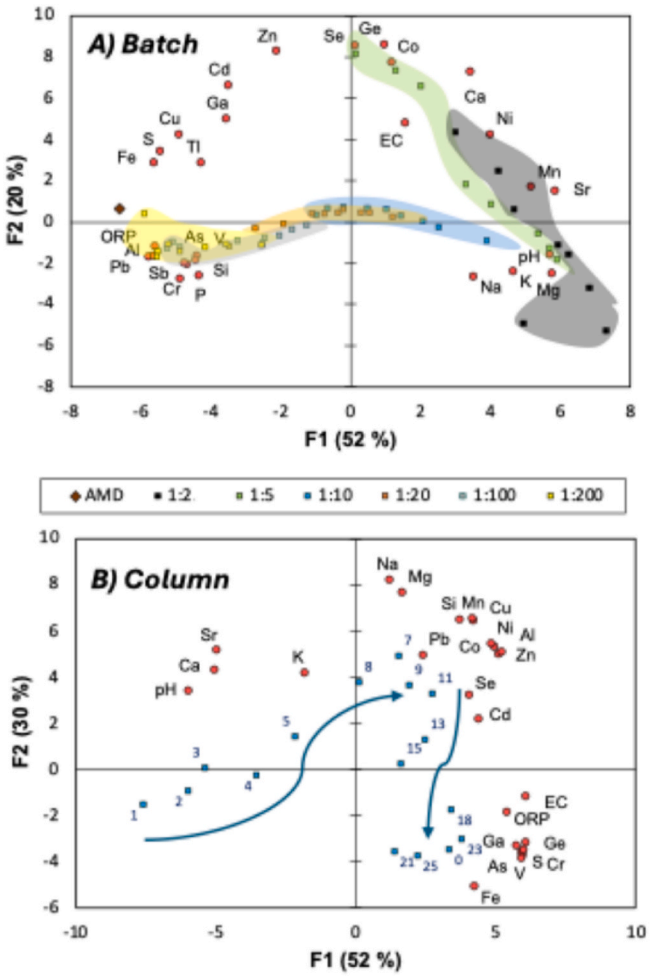

Fig. 4. Principal Component Analysis of samples collected during the batch (A) and column experiments (B).

outflow after 24 h, i.e., from 2.05 to 4.8, together with a decrease in the EC of the solution, i.e., from 14 to 7.6 mS/cm, that is, the TDS content was decreased nearly half the input value (Fig. 3). However, this tendency was reversed, with decreasing pH values until achieving initial values at the end of the experiment and increasing EC values (12.7 mS/cm at the end of the experiment). This pattern could be attributed to the progressive depletion of alkaline compounds in the BA. This fact can be inferred from the evolution of elements associated to oxides in BA. As can be seen, a fast dissolution is observed for Ca oxides (with Ca concentrations at 24 h 4.6 times higher than the initial ones) followed by the dissolution of Na and Si oxides, with concentrations 1.5 and 4.8 times higher than input waters after 7 and 11 days, respectively (Fig. 3). In the case of Al and K, the dissolution of oxides could be counterbalanced by the precipitation of secondary minerals inside the column. In this sense, a total removal of Al was observed at 24 h followed by an increase in concentration afterwards, probably until the depletion of Al oxides, when the concentration decreased again in the outflows.

The release of alkalinity from the BA led to a drastic decrease in sulfate and most metal concentrations in the first 24 h, with a removal of 100% of Cu, As, V and Ga, 99% of Pb, 73% of Fe and Cd, 64% of Zn and Co, and 60% of sulfate (Fig. 3). However, the efficiency of the column decreased progressively towards the end of the experiment, reaching similar values as in input waters, except in the case of As which maintained high removal rates (around 91%) until the end of the experiment, probably due to intense sorption processes inside the column, as it will be discussed afterwards. These sorption processes also seem to affect V and Pb. In this sense, the decrease in V removal rates was not so sharp than for the rest of the metals (>80% the first 9 days), while the removal rate of Pb increased again after 13 days, reaching high removal rates (91% of removal) at the end of the experiment (Fig. 3).

3.4. Geochemical reactions controlling metal/loid removal

A principal component analysis (PCA) was performed on both batch and column samples to infer geochemical reactions leading to sulfate and metal/loids removal during the experiments. As can be seen in Fig. 4A, the first factor explains 52% of total variance and seems to be related to the source of elements in the batch experiment. Thus, on the positive side would be located those variables preferentially provided by BA (Ca, Mg, Na, K, Sr, pH, etc) while on the negative side would be located those elements preferentially contained in AMD. The second factor explains 20% of the total variance and it would be related to the removal rate of each element during the experiment. This fact is evidenced by the grouping of the different S:L ratios around these elements. Thus, elements placed on the positive side of F2 (e.g., Fe, Cu, S, Cd or Zn) would be successfully removed using only the high ratios (1:2 and 1:5) while those located on the negative side would be removed, at variable rates, using all ratios. The alignment of samples (at different times, 15 min, 1 h, 3 h, 6 h, 12 h, 24 h, 48 h and 96 h) on the PCA for each ratio would indicate the success removing elements contained in those groups above commented. In the case of the PCA performed on column experiment samples, the first factor explains 50% of variance and seems to be related to the abundance of these elements in outflows, as can be inferred from the alignment of samples on the PCA (Fig. 4B). As can be seen, an increase in pH and enrichment of Ca, Sr and K of outflow waters is observed the first 5 days of experiment as a result of oxides dissolution. Afterwards, the dissolution of less soluble oxides (Si, Al, Mg, and Na) and the decrease in alkalinity caused the increase in concentration of most elements (Mn, Cu, Ni, Zn, Co or Pb), during the second week. Finally, the concentration of sulfate and other elements such as Fe, As, V or Cr decreased at the end of the experiment (Fig. 4B).

The second factor explains 30% of variance and it could be related to the affinity of elements to precipitate in mineral phases. Thus, Fe and S are located together due likely to the precipitation of Fe oxyhydroxisulfates and close to other elements (e.g., As, V, Cr, or Pb) known to be strongly affected by sorption processes on these phases (Acero et al., 2006; Kay et al., 2011; Larsson et al., 2017). The fluctuations in concentration observed for K during the column experiment (Fig. 3) could indicate the occurrence of dissolution of K oxides and the precipitation of jarosite, especially at the end of the experiment, when very low pH values may favor its precipitation.

Fig. 5 shows the saturation indices (SI) of samples during the batch experiments. As can be seen, all batch samples suggest jarosite and schwertmannite (especially at ratios 1:2 and 1:5) precipitation. Both mineral phases tend to control not only Fe solubility in acidic systems but also other metals such as Cu, Zn, Cd, or Pb by coprecipitation (Nordstrom and Alpers, 1999). These processes can persist event at pH values near 8 if Fe concentration exceeds that of Mn (Kaur et al., 2018). Sorption processes onto these minerals, positively charged at acidic conditions, are commonly observed for other elements found as oxyanions at acidic pH values such as or V (Acero et al., 2006; Larsson et al., 2017). Fig. S3 shows the speciation of As provided by PHREEQC code, which evidences that As was mainly found as oxyanions ($H_2AsO_4^-$ and $HAsO_4^{2-}$) during the batch experiment, especially at higher S:L ratios. This explains the higher performance achieved for As in all ratios compared to some base metals such as Cu, Zn, or Cd, where precipitation is mainly achieved at circumneutral or alkaline pH values. In addition to Fe precipitation, the removal of Al at pH values above 4 is another important process responsible of metal removal in AMD systems (Bigham and Nordstrom, 2000). Although oversaturation with respect to some Al minerals (i.e., basaluminite, and alunite) was observed for most ratios, pH values above 4 were only reached by the higher S:L ratios. Then, it is remarkable the successful removal of Al using the ratios 1:10

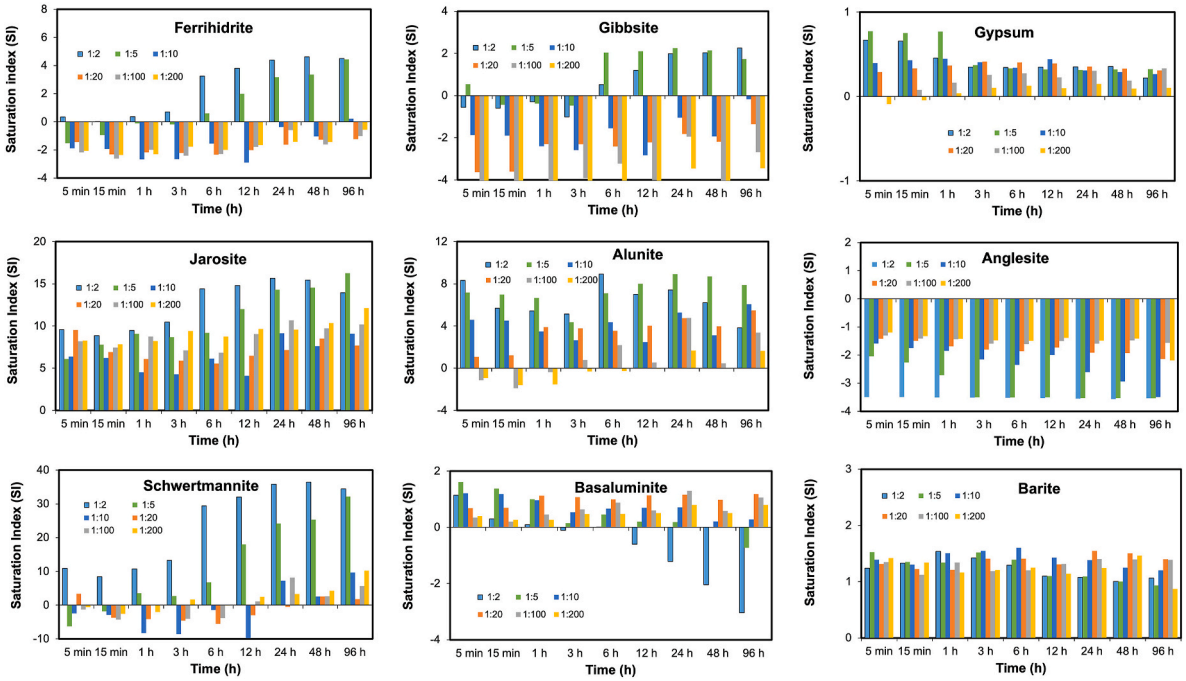

Fig. 5. Saturation indices (SI) of batch outflows with respect to main sulfate, Fe and Al minerals commonly found in AMD environments. SI values > 0 would indicate mineral precipitation while values < 0 would indicate dissolution (if present in the medium).

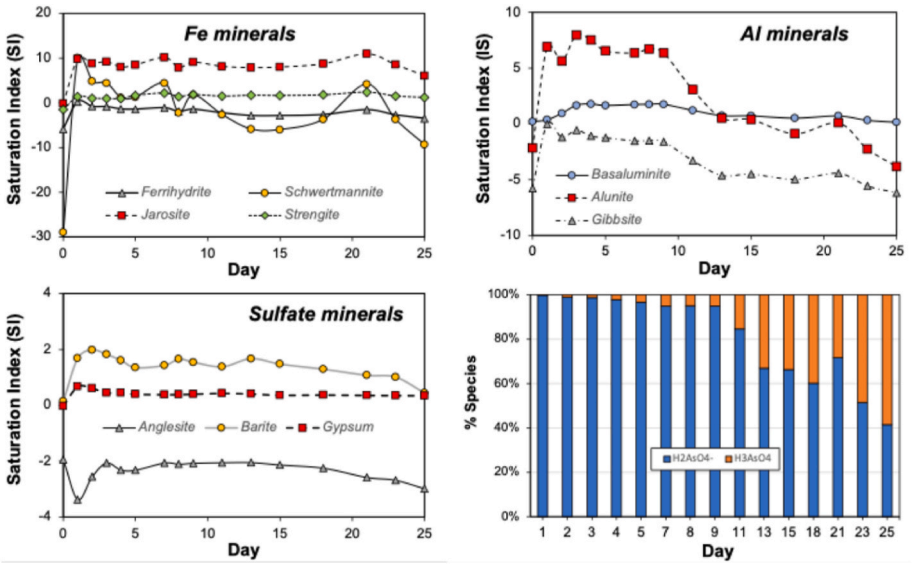

Fig. 6. Saturation indices (SI) of column outflows with respect to main sulfate, Fe and Al minerals commonly found in AMD environments, and As speciation provided by PHREEC code. SI values > 0 would indicate mineral precipitation while values < 0 would indicate dissolution (if present in the medium).

and 1:20, despite the lower pH values (Fig. 1) observed compared to the ratios 1:2 and 1:5. This fact could be explained by the affinity of Al to replace Fe in the most common Fe minerals such as schwertmannite and jarosite (e.g., Carrero et al., 2022; Grigg et al., 2024).

In the case of the column experiment, the geochemical code predicts the saturation of waters with repect jarosite and schwertmannite (mainly at the beginning of the experiment; Fig. 6). The precipitation of other mineral phases such as ettringite, alunite, basaluminite, barite and gypsum was also predicted by PHREEQC. An examination by FESEM of column materials after the experiments supports the information obtained through the geochemical code. As can be seen in Figs. S4–S6 it predominates the precipitation of Fe oxyhydroxysulfates, Fe oxides and other metals oxides which coated the surface of Si oxides remnant in BA, while other oxides (e.g., CaO, K_2O) originally present in BA, disappeared. According to the Fe/S ratio provided by FESEM, these Fe oxyhydroxysulfates would generally correspond to schwertmannite, although ratios close to those of jarosite were also observed. The analysis provided by FESEM identified the presence of Al in these Fe minerals, which could explain the removal of Al during the experiments (Figs. S5 and S6), even at pH values lower than 4. In addition, the presence of different sulfates, mainly gypsum and to a lesser extent anglesite and barite, were also identified through the column. The precipitation of these minerals, together with Fe and Al oxyhydroxysulfates may account for the sulfate removal during the experiments. To sum up, the removal of metal (loid)s during the batch and column experiments could be explained by two different processes: i) the precipitation of Fe mineral

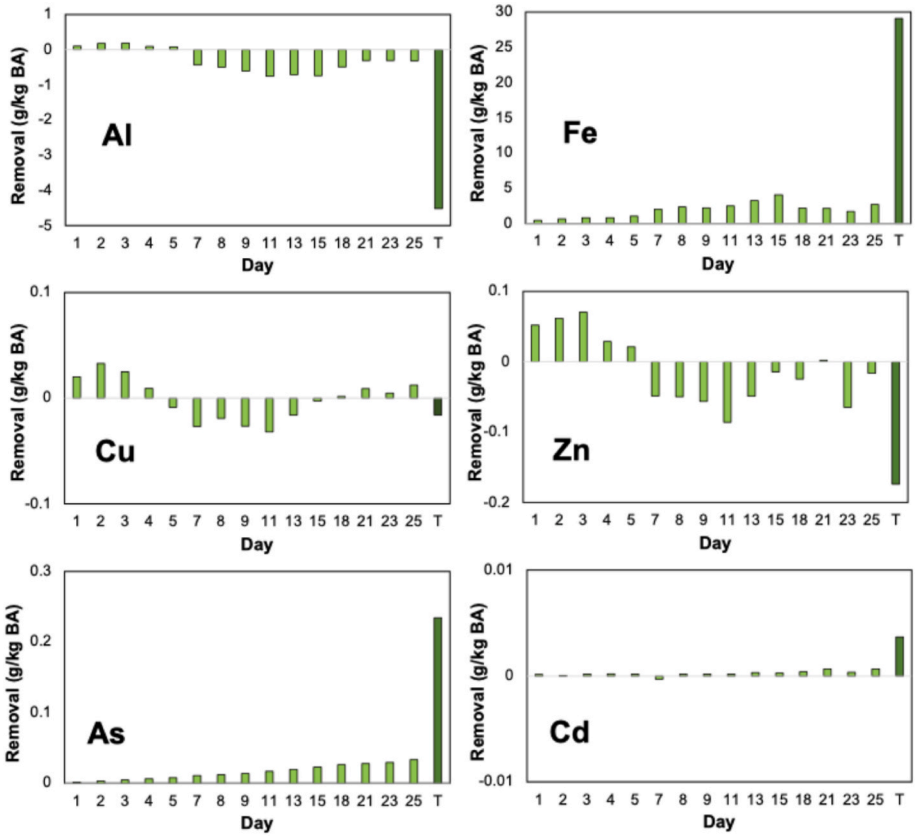

Fig. 7. Removal of metal/loids during the column experiments normalizing the amount of BA used. The dark bar represents the total amount of metal/loids eliminated.

phases (i.e., jarosite and schwertmannite) as a consequence of the increase in pH values, which may remove other metal (loid)s by coprecipitation and, ii) sorption processes onto these secondary minerals, especially those found as oxyanions like As, which may be preferentially retained in the surface of these minerals. The precipitation of secondary minerals predominates during the increases in pH values derived from the alkalinity released during BA dissolution. However, once this alkalinity is depleted, sorption becomes the prevailing mechanism of metal (loid) removal.

3.5. Environmental and technical implications

The lifetime of optimal performance of the column comprised around 5 days, when the metal concentrations started an increasing tendency, except for As. In the case of pH, the improvement only lasts 1 day, due to the depletion of alkalinity from BA. Concerning the total removal of metal/loids from AMD and its accumulation in the column, it is estimated that after the experiment around 29 g of Fe and 0.23 g of As per kg of BA (Fig. 7) were accumulated in the column, while the removal of Cd was negligible. In the case of Al and to a lesser extent Cu and Zn, the net flux was negative, that is, these elements were enriched in solution (Fig. 7). The amount of metal/loids removed from AMD per kg of BA used during the batch experiments was noticeably higher than that observed in the column experiment, reaching maximum values of 99 g of Fe, 5.0 of Cu, 3.6 g of Zn, 0.46 g of As and 0.14 g of Cd per kg of BA (Fig. 8). It is remarkable that despite achieving the worst quality of output waters, the S:L ratio 1:200 reported the highest removal rates per mass of BA. This opens the door to improve the treatment system through the implementation of sequential tanks where the polishing of water would take place until approaching the threshold values proposed by the environmental guidelines.

Although BA is currently considered as a waste during the generation of electricity from biomass burning, and therefore purchase costs may be not a limiting factor, the costs related to the transport of BA from the power plant to the remediation site needs to be considered. Obviously, for the sake of cost-efficiency the BA generated from closer sources should be used. In this study, the BA used was of S type (Vassilev et al., 2013), rich in Si, Al, Fe, Na and Ti oxides, and a high acid tendency, which provides a lower potential to treat AMD waters compared to others low and/or medium acid tendency types such as C, PK and mixed types (Bogush et al., 2019). Despite that, the removal rates obtained in this study, especially during the batch experiments, are remarkable, with values above 90% for Fe, Cu, Zn and As. Therefore, the application of other BA with low and/or medium acid tendency would improve the efficiency of the AMD treatment.

These results open the door to the use of other waste materials. For example, Nuñez-Gómez et al. (2019) performed continuous-flow studies using shrimp shell as a biomaterial for AMD treatment, reaching removal up to 90% for Fe and 88% for Mn, and a pH increase from 3.49 to 6.77. Jeremias et al. (2020) followed a similar approach using egg shells and reaching a total removal of Fe and Al, and 58% of Mn. Gonçalves et al. (2024) used fixed bed columns filed with red mud/fly ash-based geopolymeric spheres, which achieved a removal higher than 95% for Fe and between 51 and 80% for Zn, Cu, Co, Pb and Ni.

4. Conclusions

This study assessed the use of biomass ash (BA) as a neutralizing agent for treating acid mine drainage (AMD), a highly acidic and metal-rich effluent from abandoned mines, through batch and column experiments. In batch experiments, BA effectively increased the pH of AMD, particularly at higher solid-to-liquid (S:L) ratios, raising the pH from 1.9 to 7.3 and 6.4, respectively, due to BA's alkalinity. This pH rise resulted in the removal of significant amounts of dissolved metals and sulfate,

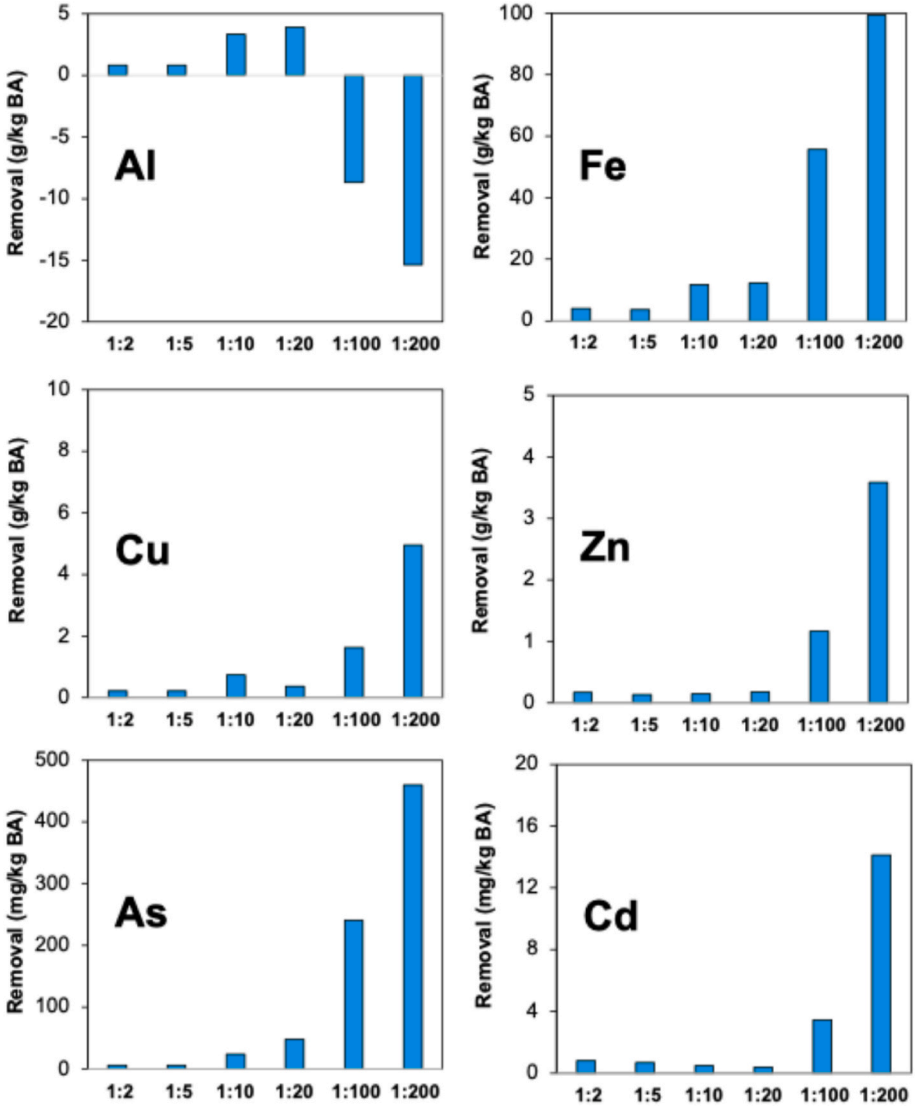

Fig. 8. Removal of metal/loids for each ratio during batch experiments normalizing the amount of BA used.

with removal efficiencies of 89–99% for Fe, 99% for Al. Cu and As, 75–99% of Pb or 66–68% for sulfate, which decreased with the depletion of alkalinity.

In column experiments, pH increased from 2.05 to 4.8 after 24 h, with total dissolved solids (TDS) decreasing by half. However, over time, pH values returned to their initial levels, and TDS increased as BA's alkaline compounds were depleted. Initially, removal efficiencies were high, achieving 100% removal of Cu, As, V, and Ga, 99% for Pb, 73% for Fe and Cd, 64% for Zn and Co, and 60% for sulfate. Nevertheless, efficiency declined over time, with most removal rates approaching baseline levels by the experiment's end, except for As (91% removal) and, to a lesser extent, Pb and V.

Geochemical and mineralogical analyses revealed that the precipitation of schwertmannite and jarosite played a key role in metal and sulfate removal. These positively charged minerals promoted the sorption of negatively charged oxyanions, explaining the high removal rates for As and V, while base metals like Cu, Zn, and Cd were less effectively removed due to their precipitation occurring at neutral to alkaline pH.

CRediT authorship contribution statement

Carlos R. Cánovas: Writing – review & editing, Writing – original draft, Visualization, Methodology. **Gerardo A. Amaya-Yaeggy:** Writing – review & editing, Validation, Formal analysis. **Dileesha Jayahansani Kotte-Hewa:** Writing – review & editing, Validation, Formal analysis. **Rafael Pérez-López:** Writing – review & editing, Supervision, Investigation, Funding acquisition, Conceptualization. **Francisco Macías:** Writing – review & editing, Supervision, Investigation, Conceptualization. **Rafael León:** Writing – review & editing, Investigation, Conceptualization. **José Miguel Nieto:** Writing – review & editing, Supervision, Investigation, Funding acquisition, Conceptualization. **María Dolores Basallote:** Writing – review & editing, Supervision, Investigation, Funding acquisition.

Declaration of competing interest

The authors declare that they have no known competing financial interests or personal relationships that could have appeared to influence the work reported in this paper.

Acknowledgements

This work was supported by the research projects ARCHENICAL and ARCHENICAL 2.0 funded by the ATLANTIC COPPER Cátedra. M.D. Basallote thanks the Regional Government of Andalusia for the EMERGIA grant (EMC21_00363) and MCIN for the RYC 2022-035326-I grant

funded by MCIN/AEI/10.13039/501100011033 and FSE+. C.R Cánovas thanks the Spanish Ministry of Science and Innovation for the Postdoctoral Fellowship granted under application reference RYC 2019-027949-I funded by MCIN/AEI/10.13039/501100011033. The authors would also like to thank to the Editor and four anonymous reviewers for the support and comments that notably improved the quality of the original paper.

Appendix A. Supplementary data

Supplementary data to this article can be found online at https://doi.org/10.1016/j.jclepro.2025.144679.

Data availability

Data will be made available on request.

References

Acero, P., Ayora, C., Torrentó, C., Nieto, J.M., 2006. The behavior of trace elements during schwertmannite precipitation and subsequent transformation into goethite and jarosite. Geochem. Cosmochim. Acta 70, 4130–4139. https://doi.org/10.1016/j.gca.2006.06.1367.

Akcil, A., Koldas, S., 2006. Acid Mine Drainage (AMD): causes, treatment and case studies. J. Clean. Prod. 14, 1139–1145. https://doi.org/10.1016/j.jclepro.2004.09.006.

Bigham, J.M., Nordstrom, D.K., 2000. Iron and aluminium hydroxysulfate minerals. In: Alpers, C.N., Jambor, J.L., Nordstrom, D.K. (Eds.), Sulfate Minerals. Crystallography, Geochemistry and Environmental Significance. Reviews in Mineralogy and Geochemistry. Mineralogical Society of America, Washington D.C, pp. 351–403.

Bogush, A.A., Dabu, C., Tikhova, V.D., Kim, J.K., Campos, L.C., 2019. Biomass ashes foracid mine drainage remediation. Waste and Biomass Valorization 11 (9), 4977–4989. https://doi.org/10.1007/s12649-019-00804-9.

Cai, J.B., 2015. Research on the treatment method of acid mine water in coal mine. Guangdong Technol 24 (18), 43–50.

Cánovas, C.R., Macías, F., Olías, M., 2018. Hydrogeochemical behavior of an anthropogenic mine aquifer: implications for potential remediation measures. Sci. Total Environ. 636, 85–93. https://doi.org/10.1016/j.scitotenv.2018.04.270.

Carrero, S., Fernandez-Martinez, A., Perez-Lopez, R., Cama, J., Dejoie, C., Nieto, J.M., 2022. Effects of aluminum incorporation on the schwertmannite structure and surface properties. Environ. Sci. Process Impacts 24, 1383–1391. https://doi.org/10.1039/D2EM00029F.

Davis, J.C., 2002. Statistics and Data Analysis in Geology. John Wiley & Sons, USA.

Ficklin, W.H., Plumlee, G.S., Smith, K.S., McHugh, J.B., 1992. Geochemical classification of mine drainages and natural drainages in mineralized areas. In: Proceedings of the 7th International Symposium on Water Rock Interaction, pp. 381–384 (Park City, Utah).

Gonçalves, N.P.F., Almeida, M.M., Labrincha, J.A., Novais, R.M., 2024. Effective acid mine drainage remediation in fixed bed column using porous red mud/fly ashcontaining geopolymer spheres. Sci. Total Environ. 940, 173633. https://doi.org/10.1016/j.scitotenv.2024.173633.

Gotore, O., Watanabe, M., Okano, K., Miyata, N., Katayama, T., Yasutaka, T., Semoto, Y., Hamai, T., 2025. Effects of batch and continuous-flow operation on biotreatment of Mn(II)-containing mine drainage. J. Environ. Sci. 152, 401–415. https://doi.org/10.1016/j.jes.2024.05.038.

Grigg, A.R.C., Notini, L., Kaegi, R., Thomas Arrigo, L.K., Kretzschmar, R., 2024. Aluminium substitution affects jarosite transformation to iron oxyhydroxides in the presence of aqueous Fe(II). Geochem. Cosmochim. Acta 374, 72–84. https://doi.org/10.1016/j.gca.2024.04.008, 2024.

He, X.W., Zhang, X.H., Li, F.Q., Zhang, C.H., 2018. Comprehensive utilization system and technological innovation of water resources in coal mines. Coal Sci. Technol. 46 (9), 4–11.

Jeremias, T.C., Pineda-Vásquez, T., Lapolli, F.R., Lobo-Recio, M.Á., 2020. Use of eggshell as a low-cost biomaterial for coal mine-impacted water (MIW) remediation: characterization and statistical determination of the treatment conditions. Water Air Soil Pollut. 231, 562. https://doi.org/10.1007/s11270-020-04919-x.

Johnson, D.B., Hallberg, K.B., 2005. Acid mine drainage remediation options: a review. Sci. Total Environ. 338, 3–14. https://doi.org/10.1016/j.scitotenv.2004.09.002.

Kaur, G., Couperthwaite, S.J., Hatton-Jones, B.W., Millar, G.J., 2018. Alternative neutralisation materials for acid mine drainage treatment. J. Water Proc. Eng. 22, 46–58. https://doi.org/10.1016/j.jwpe.2018.01.004.

Kay, R.T., Groschen, G.E., Cygan, G., Dupré, D.H., 2011. Diel cycles in dissolved barium, lead, iron, vanadium, and nitrite in a stream draining a former zinc smelter site near Hegeler, Illinois. Chem. Geol., Diel Biogeochemical Processes in Terrestrial Waters 283, 99–108. https://doi.org/10.1016/j.chemgeo.2010.10.009.

Kotte-Hewa, D.J., Durce, D., Salah, S., Cánovas, C.R., Smolders, E., 2023. Remediation of acid mine drainage and immobilization of rare earth elements: comparison between natural and residual alkaline materials. Appl. Geochem. 158, 105800. https://doi.org/10.1016/j.apgeochem.2023.105800.

Larsson, M.A., Hadialhejazi, G., Gustafsson, J.P., 2017. Vanadium sorption by mineral soils: development of a predictive model. Chemosphere 168, 925–932. https://doi.org/10.1016/j.chemosphere.2016.10.117.

Macías, F., Caraballo, M.A., Rötting, T.S., Pérez-López, R., Nieto, J.M., Ayora, C., 2012. From highly polluted Zn-rich acid mine drainage to non-metallic waters: implementation of a multi-step alkaline passive treatment system to remediate metal pollution. Sci. Total Environ. 433, 323–330. https://doi.org/10.1016/j.scitotenv.2012.06.084.

Millán-Becerro, R., Pérez-López, R., Macías, F., Cánovas, C.R., 2020. Design and optimization of sustainable passive treatment systems for phosphogypsum leachates in an orphan disposal site. J. Environ. Manag. 275, 111251. https://doi.org/10.1016/j.jenvman.2020.111251.

Moreno-González, R., Cánovas, C.R., Olías, M., Macías, F., 2020. Seasonal variability of extremely metal rich acid mine drainages from the Tharsis mines (SW Spain). Environ. Pollut. 259. https://doi.org/10.1016/j.envpol.2019.113829.

Naidu, G., Ryu, S., Thiruvenkatachari, R., Choi, Y., Jeong, S., Vigneswaran, S., 2019. A critical review on remediation, reuse, and resource recovery from acid mine drainage. Environ. Pollut. 247, 1110–1124. https://doi.org/10.1016/j.envpol.2019.01.085.

Nieto, J.M., Sarmiento, A.M., Canovas, C.R., Olias, M., Ayora, C., 2013. Acid mine drainage in the Iberian Pyrite Belt: 1. Hydrochemical characteristics and pollutant load of the Tinto and Odiel rivers. Environ. Sci. Pollut. Res. 20, 7509–7519. https://doi.org/10.1007/s11356-013-1634-9.

Nordstrom, D.K., Wilde, F.D., 1998. Reduction–oxidation potential (electrode method). National FieldManual for the Collection ofWater Quality Data. U.S. Geological Survey Techniques of Water-resources Investigations 20. U.S. Geological Survey, Reston, Va (book 9, chapter 6.5.

Nordstrom, D.K., Alpers, C.N., 1999. Geochemistry of acid mine waters. The environmental geochemistry of mine waters, 6A. Rev. Econ. Geol. 133–160.

Núñez-Gómez, D., Rodrigues, C., Lapolli, F.R., Lobo-Recio, M.A., 2019. Adsorption of heavy metals from coal acid mine drainage by shrimp shell waste: isotherm and continuous-flow studies. J. Environ. Chem. Eng. 7 (1), 102787. https://doi.org/10.1016/j.jece.2018.11.032.

Parkhurst, D.L., Appelo, C.A.J., 2013. Description of Input and Examples for PHREEQC Version 3—A Computer Program for Speciation, Batch-Reaction, One-Dimensional Transport, and Inverse Geochemical Calculations. U.S. Geological Survey Techniques and Methods, p. 497. https://doi.org/10.3133/tm6A43 book 6, chap. A43.

Romero-Matos, J., Cánovas, C.R., Macías, F., Pérez-López, R., León, R., Millán-Becerro, R., Nieto, J.M., 2023. Wildfire effects on the hydrogeochemistry of a river severely polluted by acid mine drainage. Water Res. 233, 119791. https://doi.org/10.1016/j.watres.2023.119791.

Vassilev, S.V., Baxter, D., Andersen, L.K., Vassileva, C.G., 2013. An overview of the composition and application of biomass ash. Part 1. Phase–mineral and chemical composition and classification. Fuel 105, 40–76. https://doi.org/10.1016/j.fuel.2012.09.041, 2013.

Yu, J.Y., Heo, B., Choi, I.K., Cho, J.P., Chang, H.W., 1999. Apparent solubilities of schwertmannite and ferrihydrite in natural stream waters polluted by mine drainage. Geochem. Cosmochim. Acta 63, 3407–3416. https://doi.org/10.1016/S0016-7037(99)00261-6.

Ziemkiewicz, P., Skousen, J., Simmons, J., 2003. Long-term performance of passive acid mine drainage treatment systems. Mine Water Environ. 22, 18–129. https://doi.org/10.1007/s10230-003-0012-0.